Intratumoral Heterogeneity of Glioblastoma Infiltration Revealed by Joint Histogram Analysis of Diffusion Tensor Imaging

Chao Li, MD [1,2], Shuo Wang, Bsc[3], Jiun-Lin Yan, MD PhD[1,4,5], Rory J. Piper, MRCS[1], Hongxiang Liu, PhD FRCPath[6], Turid Torheim, PhD[7,8], Hyunjin Kim, PhD[7], Jingjing Zou, PhD[9], Natalie R. Boonzaier, PhD[1,10], Rohitashwa Sinha, MRCS[1], Tomasz Matys, MD PhD[3,11], Florian Markowetz, PhD[7,8], and Stephen J. Price, PhD FRCS[1,12]

[1]Cambridge Brain Tumor Imaging Laboratory, Division of Neurosurgery, Department of Clinical Neurosciences, University of Cambridge, Addenbrooke's Hospital, Cambridge, UK
[2]Department of Neurosurgery, Shanghai General Hospital (originally named "Shanghai First People's Hospital"), Shanghai Jiao Tong University School of Medicine, China
[3]Department of Radiology, University of Cambridge, Cambridge, UK
[4]Department of Neurosurgery, Chang Gung Memorial Hospital, Keelung, Taiwan
[5]Chang Gung University College of Medicine, Taoyuan, Taiwan
[6]Molecular Malignancy Laboratory, Hematology and Oncology Diagnostic Service, Addenbrooke's Hospital, Cambridge, UK
[7]Cancer Research UK Cambridge Institute, University of Cambridge, Cambridge,
[8]CRUK & EPSRC Cancer Imaging Centre in Cambridge and Manchester, Cambridge, UK
[9]Statistical laboratory, Centre for Mathematical Sciences, University of Cambridge, UK
[10]Developmental Imaging and Biophysics Section, Institute of Child Health, University College London, London, UK
[11]Cancer Trials Unit Department of Oncology, Addenbrooke's Hospital, Cambridge, UK
[12]Wolfson Brain Imaging Centre, Department of Clinical Neurosciences, University of Cambridge, Cambridge, UK

Corresponding author: Chao Li
Email: cl109@outlook.com

Funding

National Institute for Health Research (NIHR) Clinician Scientist Fellowship (NIHR/CS/009/011, SJP); Cancer Research UK core grant (C14303/A17197 and A19274, FM lab); Cambridge Trust and China Scholarship Council (CL & SW); Chang Gung Medical Foundation and Chang Gung Memorial Hospital, Keelung, Taiwan (JLY); Cancer Research

UK & Engineering and Physical Sciences Research Council Cancer Imaging Centre in Cambridge & Manchester (C197/A16465, FM & TT); Royal College of Surgeons of England (RS); NIHR Cambridge Biomedical Research Centre (TM & SJP). This article presents independent research funded by the National Institute for Health Research (NIHR). The views expressed are those of the author(s) and not necessarily those of the NHS, the NIHR or the Department of Health.

Abstract

Background: Glioblastoma is a heterogeneous disease characterized by its infiltrative growth, rendering complete resection impossible. Diffusion tensor imaging (DTI) shows potential in detecting tumor infiltration by reflecting microstructure disruption.

Objective: To explore the heterogeneity of glioblastoma infiltration using joint histogram analysis of DTI, to investigate the incremental prognostic value of infiltrative patterns over clinical factors, and to identify specific subregions for targeted therapy.

Methods: A total of 115 primary glioblastoma patients were prospectively recruited for surgery and preoperative magnetic resonance imaging. The joint histograms of decomposed anisotropic and isotropic components of DTI were constructed in both contrast-enhancing and non-enhancing tumor regions. Patient survival was analyzed with joint histogram features and relevant clinical factors. The incremental prognostic values of histogram features were assessed using receiver operating characteristic curve analysis. The correlation between the proportion of diffusion patterns and tumor progression rate was tested using Pearson correlation.

Results: We found that joint histogram features were associated with patient survival and improved survival model performance. Specifically, the proportion of non-enhancing tumor subregion with decreased isotropic diffusion and increased anisotropic diffusion was correlated with tumor progression rate (P = .010, r = 0.35), affected progression-free survival (hazard ratio = 1.08, P < .001), and overall survival (hazard ratio = 1.36, P < .001) in multivariate models.

Conclusion: Joint histogram features of DTI showed incremental prognostic values over clinical factors for glioblastoma patients. The non-enhancing tumor subregion with decreased isotropic diffusion and increased anisotropic diffusion may indicate amore infiltrative habitat and potential treatment target.

Short title: Heterogeneity of Glioblastoma Infiltration

Key words: Glioblastoma; Tumor infiltration; Magnetic Resonance Imaging; Survival; Diffusion Tensor Imaging; Heterogeneity.

Introduction

Glioblastoma is the commonest primary malignant tumor in the central nervous system in adults and is amongst the most lethal cancers.[1] It is characterized by its diffuse infiltration into the normal brain,[2] which renders total resection impossible. Progression after surgery is therefore almost inevitable, and typically occurs adjacent to the resection cavity.[3]

Glioblastoma is an extensively heterogeneous disease. Recent genomic findings have revealed that multiple clones co-exist in the same tumor.[4, 5] It is recognized that glioblastoma is also heterogeneous in its infiltrative pattern. Migratory clones within the tumor may result in a more infiltrative phenotype, which may be especially responsible for treatment failure.[3] Previous study showed that the migratory phenotype of a subset of cells can predict tumor recurrence.[6] Understanding the intratumoral heterogeneity of glioblastoma infiltration is of clinical significance for targeted surgery and radiotherapy.

Magnetic resonance imaging (MRI) has unique advantages in understanding spatial structural variations within glioblastoma. Current clinical management is primarily based on structural sequences, among which the post-contrast T1-weighted imaging is most widely-used. This approach, however, provides limited quantitative information about tumor infiltration. Other sequences, such as fluid attenuated inversion recovery (FLAIR), although integrated in clinical assessment,[7] is still considered to be non-specific for differentiating tumor infiltration from edema and delayed radiation white matter change.[8]

Diffusion tensor imaging (DTI) is a method that measures the magnitude and direction of water molecule movement, and has been shown to be sensitive in detecting tumor infiltration.[9] Glioblastoma may preferentially migrate along white matter tracts and cause disruption.[10] The diffusion of water molecules in tumor and peritumoral brain is consequently altered. By decomposing the tensor into isotropic (DTI-p) and anisotropic (DTI-q) components, the directional diffusion can be measured.[11] This approach has been found useful in predicting tumor progression and patient survival.[12, 13] It remains to be discovered, however, whether integrating these components can offer a more comprehensive measure of tumor infiltration. Furthermore, molecular biomarkers, such as isocitrate dehydrogenase (IDH) mutations[14] and oxygen 6–methylguanine-DNA methyltransferase (MGMT) promoter methylation,[15] are reported to be of diagnostic and prognostic significance for glioblastoma. One previous study has shown that IDH mutant glioblastoma is less invasive determined by DTI maps. [9] Whether the DTI markers, particularly DTI-p and -q, can provide additional prognostic value to molecular markers is unclear.

The purpose of this study was to explore the heterogeneity of glioblastoma infiltration using joint histogram analysis of DTI, to investigate the incremental prognostic value of infiltrative patterns over clinical factors, and to identify specific subregions that may be suitable for targeted therapy. The hypothesis was that joint histogram analysis of diffusion parameters can differentiate anatomically-defined regions into subregions with different diffusion patterns of prognostic values.

Methods

Study design

We prospectively and preoperatively recruited patients with an initial radiological diagnosis of supratentorial primary glioblastoma from July 2010 to August 2015. All patients were required to have a good performance status (World Health Organization performance status 0-1) before surgery. Exclusion criteria included history of a previous brain tumor, cranial surgery, radiotherapy/chemotherapy, or contraindication for MRI scanning. This study was approved by the local institutional review board. Signed informed consent was obtained from all patients.

Surgery

To achieve maximal safe resection, surgery was performed with the guidance of neuronavigation (StealthStation, Medtronic, Fridley, MN, USA) and 5-aminolevulinic acid fluorescence (5-ALA, Medac, Stirling, UK).

Pre-operative MRI acquisition

A 3-Tesla MRI system (Magnetron Trio; Siemens Healthcare, Erlangen, Germany) was used. Pre-operative DTI, post-contrast T1-weighted imaging, T2-weighted imaging and T2-weighted FLAIR were acquired for all the subjects pre-operatively. Sequence details are provided in Supplemental Digital Content 1. All patient underwent MRI within 72hrs postoperatively.

Imaging processing

DTI was processed with the diffusion toolbox (FDT) of FSL[16] v5.0.8 (Centre for Functional MRI of the Brain, Oxford, UK).[17] Normalization and eddy current correction were performed. DTI-p and –q were calculated using previously described equation.[11] Anatomical images were coregistered to DTI with an affine transformation, using FSL linear image registration tool (FLIRT).[18]

Tumor regions of interest (ROIs) were manually drawn on post-contrast T1-weighted and FLAIR images using 3D slicer v4.6.2[19] (Surgical Planning Laboratory, Brigham and Women's Hospital, Boston, MA, USA; www.slicer.org/) by a neurosurgeon with > 8 years of experience (CL), a researcher with > 4 years of brain tumor image analysis experience (NRB) and reviewed by a neuroradiologist with > 8 years of experience (TM). Non-enhancing ROI, defined as the non-enhancing region outside of contrast enhancement, were obtained in MATLAB (MathWorks, Natick, MA, USA) by Boolean subtraction on contrast-enhancing and FLAIR ROIs. Normal-appearing white matter (10mm in diameter) was manually segmented from the contralateral white matter and used as normal control. The region is far from the lesion and has no perceivable abnormalities. [20] Tumor volume was calculated in FSL.[17] Inter-rater reliability was tested using Dice similarity coefficient scores.

Histogram analysis

Histogram analysis were performed in the Statistics and Machine Learning Toolbox of MATLAB. Contrast-enhancing and non-enhancing ROIs were analyzed independently. A demonstration of histogram analysis is shown in Figure 1. Each voxel of DTI-p and -q in tumor ROIs was normalized by dividing it by the mean value in contralateral normal-appearing white matter. The univariate histograms of DTI-p and -q were constructed with the normalized voxels using 100 bins (Figure 1. A & B). The mean, median, 25th and 75th percentile of the histogram were calculated.

The joint histogram was constructed with x-axis and y-axis representing the normalized DTI-p and -q values respectively, using 50×50 bins on both axes (Fig 1. C). Each voxel within tumor was assigned to a corresponding bin in the 3D space, according to the DTI-p and -q values they carried. Since the voxel values were normalized as above, the coordinator point (DTI-p = 1, DTI-q = 1) was designated to represent the diffusion pattern in contralateral normal-appearing white matter, which was calculated as the mean value of DTI-p and DTI-q in the regions of interest, as described above. Thus, four voxel groups describing the co-occurrence distribution of DTI-p and -q abnormality were obtained (Fig 1. D), namely:

I. Voxel Group I (decreased DTI-p/decreased DTI-q, p↓/q↓)
II. Voxel Group II (decreased DTI-p/increased DTI-q, p↓/q↑)
III. Voxel Group III (increased DTI-p/increased DTI-q, p↑/q↑)
IV. Voxel Group IV (increased DTI-p/decreased DTI-q, p↑/q↓)

The proportion of each voxel group in the ROI were used as joint histogram features, obtained from both contrast-enhancing and non-enhancing tumor regions, providing eight features per patient.

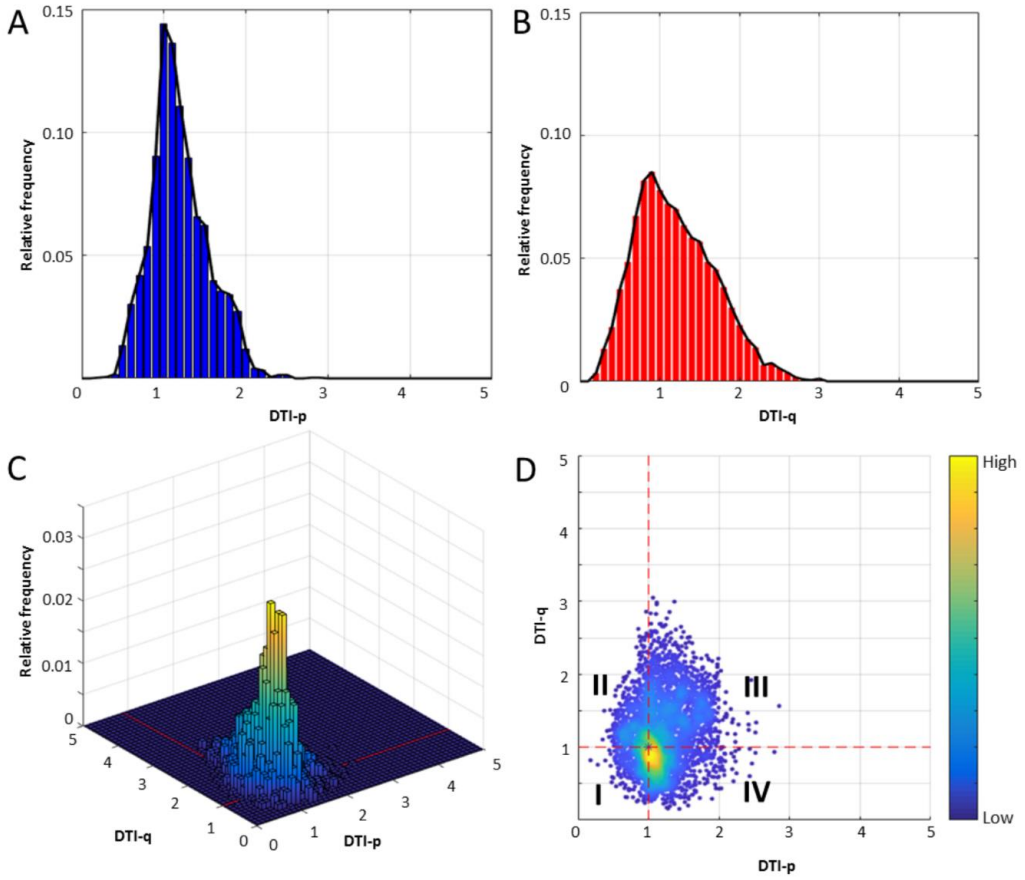

Figure 1. Illustration of the univariate and joint histogram analysis. Univariate histograms of DTI-p (A) and -q (B) were constructed using 100 bins. The joint histogram was constructed with x- and y-axis representing DTI-p and -q values using 50 × 50 bins. The bin height of the joint histogram represented the relative frequency of voxels falling into a specific DTI-p and -q range (C). Four voxel groups of DTI-p and -q abnormalities were obtained (D): I. Voxel Group I (decreased DTI-p/decreased DTI-q); II. Voxel Group II (decreased DTI-p/increased DTI-q); III. Voxel Group III (increased DTI-p/increased DTI-q); IV. Voxel Group IV (increased DTI-p/decreased DTI-q).

Assessment of IDH-1 R132H Mutation and MGMT Methylation Status

IDH-1 R132H mutation status was firstly determined using immunohistochemistry. In patients for whom IDH-1 R132H mutation was not detected, tumor DNA was extracted from tumor-rich tissue and sequenced for other rare IDH mutations. Pyrosequencing of four CpG sites of the MGMT gene was performed. A cut-off of 10% mean methylation for the four CpG sites was used to determine tumors as methylated or unmethylated.[21, 22] Assessment details are provided in Supplemental Digital Content 2.

Evaluation of treatment response and tumor progression

Extent of resection was assessed according to the post-operative MRI scans acquired within 72 hours, and were classified as complete resection, partial resection of enhancing tumor or biopsy.[23] According to their performance status, patients received adjuvant therapy post-operatively. Treatment response was evaluated according to the Response Assessment in Neuro-oncology criteria,[7] which incorporates clinical and radiological changes to identify progression. Pseudoprogression was suspected where new contrast enhancement appeared within first 12 weeks after completing chemoradiotherapy. In such cases, treatment was continued and pseudoprogression was identified where later response occurred. As a result, in some cases, true progression was determined retrospectively.

The time to tumor progression was defined as the period between surgery date and the date of first post-contrast T1-weighted images that showed progression (as determined by a consultant neuroradiologist). Available progression images were reviewed by three authors (CL, JLY and RJP). The progression volume was calculated and the progression rate was defined as progression volume normalized by time to progression. Details of progression assessment are provided in Supplemental Digital Content 3.

Statistical analysis

All statistical analyses were performed in RStudio v3.2.3 (Rstudio, Boston, MA, USA). Histogram features or tumor volume were assessed using Wilcoxon signed rank test. Survival was evaluated in patients who have received concurrent temozolomide (TMZ) chemoradiotherapy followed by adjuvant TMZ post-operatively. Cox proportional hazards regression was performed, accounting for relevant covariates, including IDH-1 mutation, MGMT methylation, sex, age, extent of resection and contrast-enhancing tumor volume. Patients who were alive at the last known follow-up were censored. For Kaplan-Meier analysis, continuous variables were dichotomized using optimal cutoff values, calculated by the R Package "survminer" (https://cran.r-project.org/web/packages/survminer/). Logistic regression models were used to test prognostic values of covariates for 12-, and 18-month overall survival (OS) and progression-free survival (PFS). The baseline models were firstly constructed using all above relevant clinical covariates. Specific histogram features were then added one by one into the baseline model to assess their incremental prognostic value, by comparing the area under the receiver operator characteristics curve (AUC) using one-way ANOVA. To select prognostic variables, multivariate Cox regression was performed, using forward and backward

stepwise procedures. The forward procedure started from the model containing only one covariate and add one covariate in each step, whereas the backward procedure initiated from the model containing all covariates and delete one covariate in each step. For each step, the model was evaluated using Akaike Information Criterion (AIC). The final models were constructed using the covariates selected by this procedure. Correlations between variables were tested using Pearson correlation test. The hypothesis of no effect was rejected at a two-sided level of 0.05.

Results

Patients

We prospectively recruited 136 patients into the study. After surgery, 115 (84.6%) histologically confirmed glioblastoma patients (mean age 59.3 years, range 22 - 76 years, 87 males) were included. Clinical characteristic of 115 included patients are summarized in Table 1. Flow chart of patient recruitment is provided in Supplemental Digital Content 4.

Of the 115 patients, 84 (73.0 %) patents received concurrent temozolomide (TMZ) chemoradiotherapy followed by adjuvant TMZ, post-operatively. Other patients received a short-course radiotherapy (17.4%, 20/115) or best supportive care (9.6%, 11/115), due to their poor post-operative performance status. Survival data were available for 80 of 84 (95.2%) patients that were treated with CCRT and 4 (4.8%) patients were lost to follow up.

Regions of interest

Inter-rater reliability testing of regions of interest (ROIs) showed excellent agreement between the two raters, with Dice scores (mean ± standard deviation [SD]) of 0.85 ± 0.10 and 0.86 ± 0.10 for contrast-enhancing and non-enhancing ROIs respectively.

Table 1. Clinical characteristics	
Variable	Patient Number
Age at diagnosis	
<60	40
≥60	75
Sex	
Male	87
Female	28
Extent of resection (of enhancing tumor)	
Complete resection	77
Partial resection	32
Biopsy	6
MGMT-methylation status*	
Methylated	48
Unmethylated	63
IDH-1 mutation status	
Mutant	7
Wild-type	108
Tumor volumes(cm^3) [#]	
Contrast-enhancing	53.6 ± 33.8
Non-enhancing	62.5 ± 44.0
Survival (days)	
Median OS (range)	424 (52 -1376)
Median PFS (range)	262 (25-1130)
*MGMT-methylation status unavailable for 4 patients; [#]mean ± SD of original data. SD: standard deviation; MGMT: O-6-methylguanine-DNA methyltransferase; IDH-1: Isocitrate dehydrogenase 1; cm: centimeter; OS: overall survival; PFS: progression-free survival.	

Diffusion signatures of contrast-enhancing and non-enhancing regions

The diffusion signatures of ROIs are demonstrated in Table 2. For univariate histogram features, both contrast-enhancing and non-enhancing regions displayed increased DTI-p (all values greater than 1). A decreased DTI-q (all values less than 1) was consistently observed in contrast-enhancing region, whereas non-enhancing regions displayed increased mean and 75th percentile of DTI-q. In accordance with the univariate histogram, joint histogram analysis

showed that Voxel Group IV (increased DTI-p/decreased DTI-q, p↑/q↓) accounted for the largest proportion in tumor.

Table 2. Histogram features

Variable	contrast-enhanced region	non-enhancing region	*P* value
	Mean ± SD	Mean ± SD	
DTI-p histogram features			
25th percentile	1.18 ± 0.23	1.11 ± 0.15	< **0.001**
Median	1.47 ± 0.38	1.32 ± 0.23	**0.001**
Mean	1.57 ± 0.36	1.37 ± 0.22	< **0.001**
75th percentile	1.90 ± 0.60	1.59 ± 0.30	< **0.001**
DTI-q histogram features			
25th percentile	0.42 ± 0.14	0.71± 0.18	< **0.001**
Median	0.65 ± 0.19	0.95 ± 0.23	< **0.001**
Mean	0.71 ± 0.19	1.01 ± 0.24	< **0.001**
75th percentile	0.93 ± 0.24	1.24 ± 0.29	< **0.001**
DTI Joint histogram features (%)			
Voxel Group I	8.50 ± 10.37	5.49 ± 6.17	< **0.001**
Voxel Group II	3.83 ± 4.92	7.27 ± 8.07	< **0.001**
Voxel Group III	20.78 ± 13.65	40.33 ± 18.97	< **0.001**
Voxel Group IV	66.90 ± 16.28	46.92 ± 20.40	< **0.001**

DTI: diffusion tensor imaging; p: isotropic component; q: anisotropic component; SD: standard deviation; Voxel Group I: decreased DTI-p, decreased DTI-q (p↓/q↓,); Voxel Group II: decreased DTI-p, increased DTI-q (p↓/q↑); Voxel Group III: increased DTI-p, increased DTI-q (p↑/q↑); Voxel Group IV: increased DTI-p, decreased DTI-q (p↑/q↓).

Multivariate survival analysis

The multivariate survival model of PFS and OS were fitted in 78 patients for whom all relevant covariates were available (Table 3). Five joint histogram features were significantly associated with survivals. Specifically, higher proportions of Voxel Group II (p↓/q↑), in both contrast-enhancing and non-enhancing regions, were associated with worse survival (in contrast-enhancing region, PFS: hazard ratio [HR] = 1.06, $P = 0.036$; OS: HR = 1.09, $P = 0.004$; in non-enhancing region, PFS: HR = 1.08, $P < 0.001$; OS: HR = 1.11, $P < 0.001$). The Kaplan-Meier curves are demonstrated in Figure 2, with *P* values from Log-rank test.

Table 3. Cox multivariate modelling of survivals

Variable	Progression-free survival*			Overall survival*		
	HR	95%CI	*P* value	HR	95%CI	*P* value
Contrast-enhancing region						
Voxel Group I	1.02	0.990-1.049	0.205	1.03	1.000-1.064	**0.049**
Voxel Group II	1.06	1.004-1.128	**0.036**	1.09	1.028-1.156	**0.004**
Voxel Group III	1.01	0.989-1.025	0.449	1.01	0.988-1.028	0.432
Voxel Group IV	0.98	0.968-1.001	0.061	0.98	0.960-0.996	**0.015**
Non-enhancing region						
Voxel Group I	1.02	0.975-1.057	0.463	0.997	0.947-1.049	0.904
Voxel Group II	1.08	1.041-1.128	**<0.001**	1.11	1.064-1.165	**<0.001**
Voxel Group III	1.01	0.996-1.026	0.145	1.01	0.997-1.026	0.116
Voxel Group IV	0.98	0.969-0.996	**0.014**	0.98	0.969-0.997	**0.015**

*Cox models accounted for each histogram feature and all covariates of sex, age, extent of resection, IDH-1 mutation status, MGMT methylation status and contrast-enhancing tumor volume. MGMT: O-6-methylguanine-DNA methyltransferase; IDH-1: Isocitrate dehydrogenase 1; HR: hazard ratio; CI: confidence interval; Voxel Group I: decreased DTI-p, decreased DTI-q (p↓/q↓); Voxel Group II: decreased DTI-p, increased DTI-q (p↓/q↑); Voxel Group III: increased DTI-p, increased DTI-q (p↑/q↑); Voxel Group IV: increased DTI-p, decreased DTI-q (p↑/q↓).

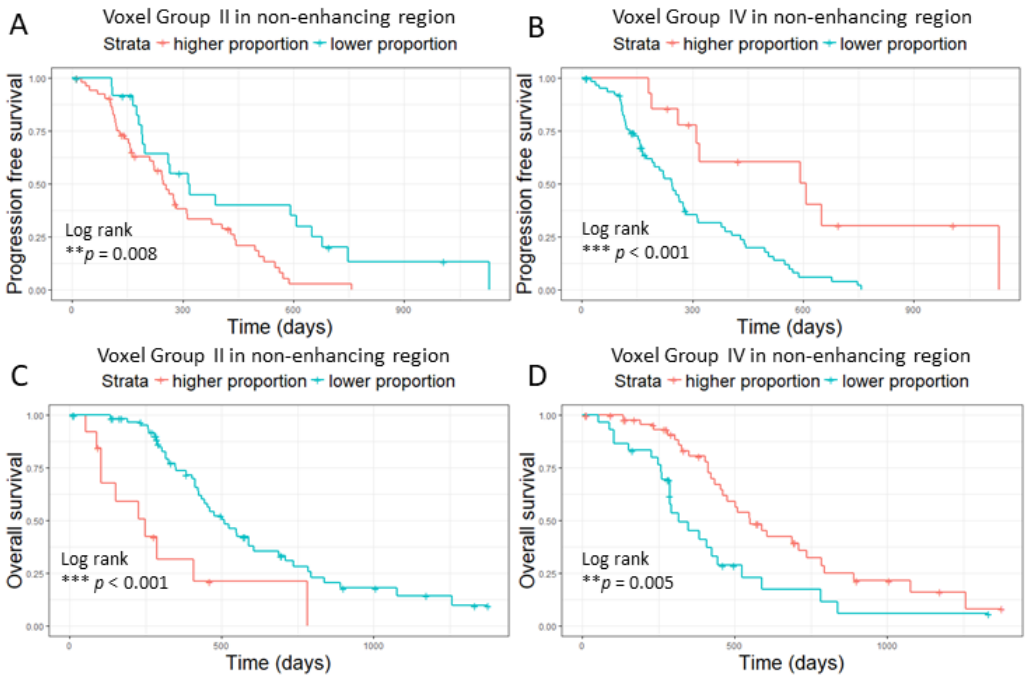

Figure 2. Kaplan-Meier plots of survival analysis. The proportions of voxel groups were dichotomized using optimal cutoff values calculated in R. Log-rank test showed higher proportion of Voxel Group II in non-enhancing tumor region was associated with worse PFS (P = 0.008, cut off value 2.3%) (A) and worse OS (P < 0.001, cut off value 12.8%) (C). Lower proportion of Voxel Group IV in non-enhancing tumor region was associated with worse PFS (P < 0.001, cut off value 65.9%) (B) and worse OS (P = 0.005, cut off value 36.9%) (D).

Incremental Prognostic Value of Joint Histogram Features

The results of model comparisons are shown in Table 4. Six joint histogram features significantly improved the model (each $P < 0.05$): Voxel group I (p↓/q↓), Voxel group II (p↓/q↑), Voxel group IV (p↑/q↓) in the contrast-enhancing region, and Voxel group II (p↓/q↑), Voxel group III (p↑/q↑), Voxel group IV (p↑/q↓) in the non-enhancing region. Particularly, Voxel Group II (p↓/q↑) in the non-enhancing region significantly improved the 12-month and 18-month survival models.

Table 4. Model Comparison						
Model	12 month AUC	95% CI	*P* value	18 month AUC	95% CI	*P* value
Progression-free survival						
baseline*	0.77	0.65-0.88		0.75	0.61-0.88	
Contrast-enhancing region						
+Voxel Group I	0.81	0.71-0.92	**0.038**	0.78	0.65-0.92	0.424
+Voxel Group II	0.80	0.70-0.91	0.153	0.86	0.76-0.96	**0.003**
+Voxel Group III	0.77	0.66-0.88	0.916	0.79	0.66-0.91	0.229
+Voxel Group IV	0.81	0.70-0.91	0.077	0.81	0.68-0.93	**0.044**
Non-enhancing region						
+Voxel Group I	0.76	0.65-0.88	0.792	0.76	0.63-0.89	0.763
+Voxel Group II	0.80	0.70-0.91	0.096	0.86	0.74-0.97	**0.017**
+Voxel Group III	0.80	0.69-0.91	0.372	0.83	0.71-0.95	**0.023**
+Voxel Group IV	0.80	0.70-0.91	0.154	0.83	0.71-0.95	**0.011**
Overall survival						
baseline*	0.81	0.70-0.93		0.71	0.58-0.83	
Contrast-enhancing region						
+Voxel Group I	0.82	0.69-0.95	0.070	0.75	0.63-0.87	0.091
+Voxel Group II	0.84	0.73-0.96	0.063	0.77	0.65-0.88	0.075
+Voxel Group III	0.81	0.70-0.93	0.746	0.73	0.60-0.85	0.443
+Voxel Group IV	0.84	0.72-0.95	0.164	0.77	0.65-0.88	**0.035**
Non-enhancing region						
+Voxel Group I	0.81	0.70-0.93	0.942	0.71	0.58-0.83	0.952
+Voxel Group II	0.84	0.72-0.96	**0.015**	0.78	0.66-0.89	**0.022**
+Voxel Group III	0.84	0.74-0.94	0.109	0.74	0.61-0.86	0.196
+Voxel Group IV	0.85	0.75-0.95	**0.019**	0.76	0.64-0.88	0.053

*Baseline models were built using sex, age, extent of resection, IDH-1 mutation status, MGMT methylation status and contrast-enhancing tumor volume. MGMT: O-6-methylguanine-DNA methyltransferase; IDH-1: Isocitrate dehydrogenase 1; AUC: area under receiver operator characteristics curve; HR: hazard ratio; CI: confidence interval; DTI: diffusion tensor imaging; Voxel Group I: decreased DTI-p, decreased DTI-q (p↓/q↓,); Voxel Group II: decreased DTI-p, increased DTI-q (p↓/q↑); Voxel Group III: increased DTI-p, increased DTI-q (p↑/q↑); Voxel Group IV: increased DTI-p, decreased DTI-q (p↑/q↓).

Stepwise Multivariate Cox Model Selection

All clinical factors and histogram features that significantly improved AUC were tested (Table 5). Significant prognostic variables for both PFS and OS included extent of resection, MGMT

methylation status and Voxel Group II (p↓/q↑) in the non-enhancing region. Specifically, Voxel Group II (p↓/q↑) in the non-enhancing region contributed to a worse PFS (HR = 1.08, $P < 0.001$) and worse OS (HR = 1.36, $P < 0.001$), and displayed a higher HR than other voxel groups.

Table 5. Stepwise Cox multivariate modelling of survivals

Variable	Progression-free survival*			Overall survival*		
	HR	95%CI	*P* value	HR	95%CI	*P* value
Sex	1.58	0.90-2.77	0.109	/	/	/
Age	/	/	/	/	/	/
Extent of resection	3.25	1.67-6.34	**0.001**	2.13	1.12-4.06	**0.022**
IDH-1 mutation status	/	/	/	/	/	/
MGMT methylation status	0.50	0.29-0.86	**0.013**	0.51	0.27-0.97	**0.040**
Contrast-enhancing volume	/	/	/	1.02	1.01-1.03	**0.001**
Voxel Group I (contrast-enhancing region)	/	/	/	1.06	1.02-1.11	**0.006**
Voxel Group II (contrast-enhancing region)	/	/	/	/	/	/
Voxel Group IV (contrast-enhancing region)	/	/	/	/	/	/
Voxel Group II (non-enhancing region)	1.08	1.04-1.13	**<0.001**	1.36	1.16-1.59	**<0.001**
Voxel Group III (non-enhancing region)	/	/	/	1.19	1.05-1.34	**0.005**
Voxel Group IV (non-enhancing region)	/	/	/	1.18	1.05-1.32	**0.005**

*All clinical factors and joint histogram features that showed incremental prognostic values in model comparisons were included into selection. Final models were built only using the covariates selected by the stepwise procedure. HR: hazard ratio; CI: confidence interval; IDH-1: Isocitrate dehydrogenase 1; MGMT: O-6-methylguanine-DNA methyltransferase; Voxel Group I: decreased DTI-p, decreased DTI-q (p↓/q↓); Voxel Group II: decreased DTI-p, increased DTI-q (p↓/q↑); Voxel Group III: increased DTI-p, increased DTI-q (p↑/q↑); Voxel Group IV: increased DTI-p, decreased DTI-q (p↑/q↓).

Correlations with tumor progression rate

The correlation with tumor progression rate was tested in 57 patients who had progression and available MR images at progression. The progression volume (mean ± SD) outside of the resection cavity was 14.3 ± 22.0 cm^3. The progression rate (mean ± SD) was 0.003 ± 0.013 cm^3/day. The results indicated that Voxel Group II (p↓/q↑) in the non-enhancing region had a significant positive correlation ($P = 0.010$, r = 0.35) with the progression rate, whereas Voxel

Group IV (p↑/q↓) in the non-enhancing region (*P* = 0.040, r = -0.28) showed a negative correlation. No significant correlations were found from other voxel groups. Two examples of pre-operative and progression images, as well as the annotated subregions of Voxel Group II and Voxel Group IV in the non-enhancing region are demonstrated in Figure 3 & Figure 4.

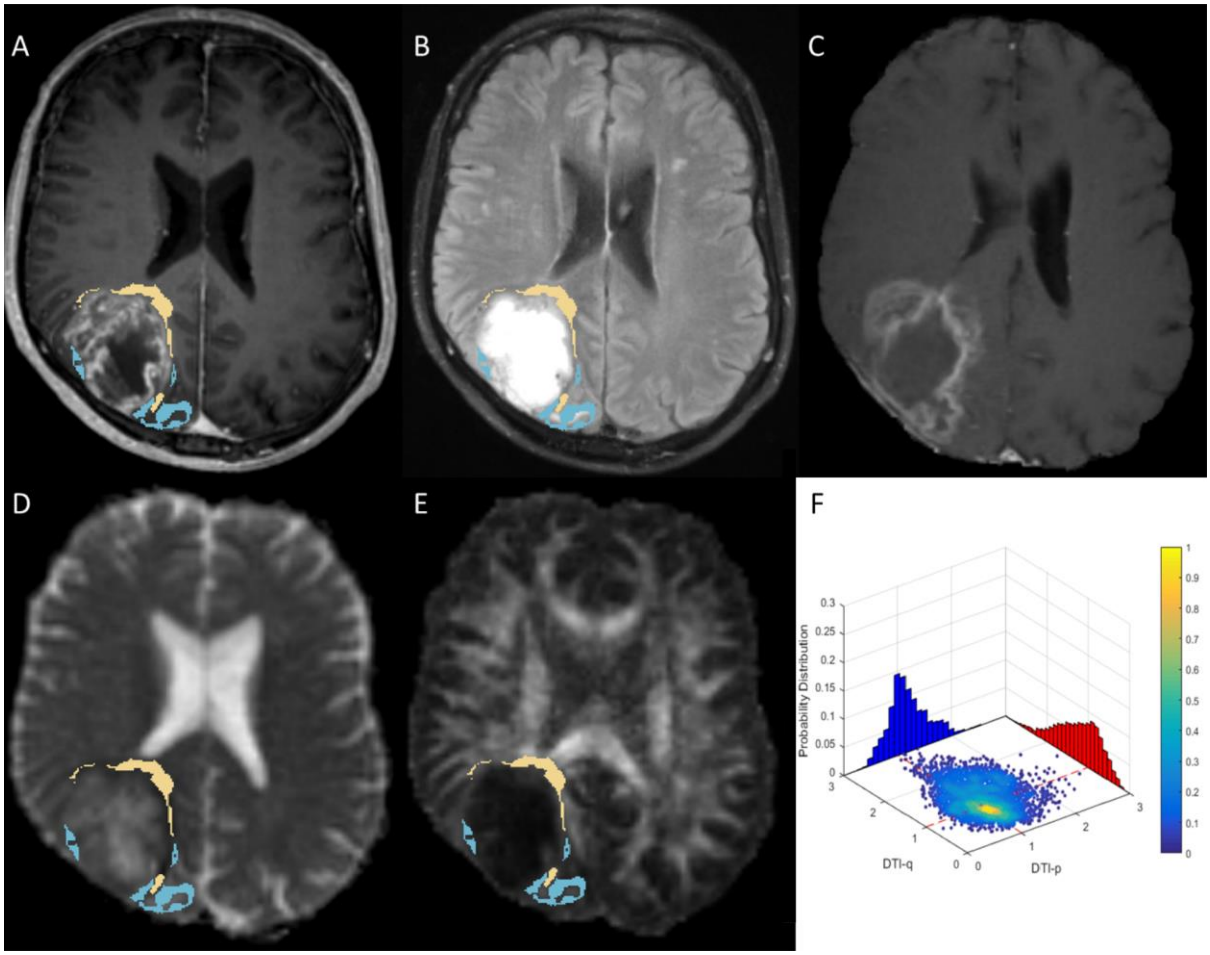

Figure 3. The Voxel Group II (yellow) and Voxel Group IV (blue) of non-enhancing in case 1. The 63-year-old man was radiologically diagnosed with primary glioblastoma (A & B). Volumetric analysis of pre-operative MRI showed contrast enhanced tumor volume was 83.6 cm^3. The patient received tumor resection with the guidance of neuronavigation and 5-aminolevulinic acid fluorescence with the aim of maximal resection, but only subtotal resection was achieved according to 72h post-operative MRI. Pathological assessment confirmed this was a MGMT-methylated glioblastoma and IDH mutation was negative. The patient received concomitant and adjuvant temozolomide chemoradiotherapy. The progression-free survival was 47 days and overall survival was 104 days. The post-contrast T1-weighted imaging showed the progression was around the resection cavity (C). Joint histogram analysis of pre-operative DTI-p (D) and DTI-q (E) maps showed Voxel Group II (yellow) occupied 15.5% in the non-enhancing tumor and Voxel Group IV (blue) occupied 28.2% of the non-enhancing tumor (F).

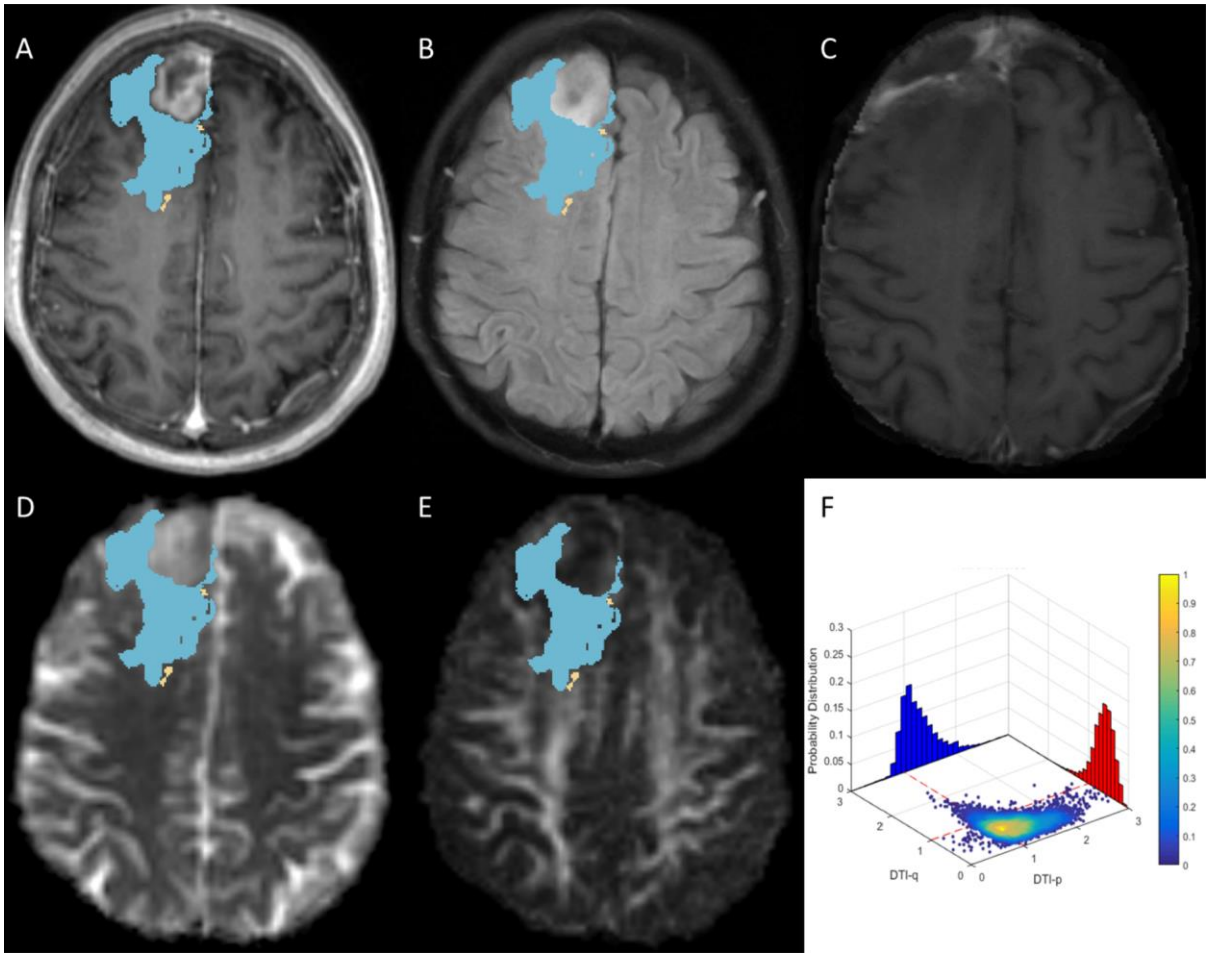

Figure 4. The Voxel Group II (yellow) and Voxel Group IV (blue) of non-enhancing in case 2. The 65-year-old man was radiologically diagnosed with primary glioblastoma (A & B). Volumetric analysis showed contrast enhanced tumor volume was 37.4 cm^3. Gross total resection was achieved in this patient with the guidance of neuronavigation and 5-aminolevulinic acid fluorescence. Pathological assessment confirmed a MGMT-methylated glioblastoma and IDH mutation was negative. The patient received concomitant and adjuvant temozolomide chemoradiotherapy. The progression-free survival was 1006 days and patient was alive in the last follow-up. Post-contrast T1-weighted imaging showed a minor progression around the resection cavity (C). Joint histogram analysis of pre-operative DTI-p (D) and DTI-q (E) maps showed Voxel Group II (yellow) occupied 2.3% of the non-enhancing tumor and Voxel Group IV (blue) occupied 81.5% of the non-enhancing tumor (F).

Discussion

In this study, we found that joint histogram analysis using DTI-p and -q can reflect the heterogeneity of glioblastoma infiltration. The histogram features obtained using this method can improve the prognostic value of IDH-1 mutation and MGMT promoter methylation status. The non-enhancing subregion with decreased DTI-p and increased DTI-q may indicate a more infiltrative tumor habitat.

Previous studies have shown that DTI has potential in studying white matter pathology and is useful in detecting tumor infiltration.[24-26] Using stereotactic biopsies, DTI-p and -q is demonstrated to distinguish gross tumor and peritumoral region.[8] As the only *in vivo* method of describing brain microstructure, it confers additional information for surgical stratification.[27, 28] However, the interpretation of the tensor is challenging due to its high dimensionality.[26] Substantial efforts have been made to simplify the tensor into scalar measures. Among these markers, fractional anisotropy (FA) and mean diffusivity (MD) are commonly used.[11] Since FA can be affected by both anisotropic and isotropic components (according to its definition equation), its utility is inconsistent. An enhanced visualization and quantification of tensor imaging was subsequently advanced by decomposing the raw tensor into isotropic (p) and anisotropic (q) components.[11] This technique has shown its utility in detecting the subtle change caused by tumor invasion and predicting progression.[9] Consistent with previous studies,[8] our univariate results showed increased DTI-p and decreased DTI-q can be found in the majority of tumor area. Additionally, the non-enhancing tumor may display increased DTI-q, which was not observed in contrast-enhancing region and may characterize the infiltrative region.

Previous studies have shown that histogram features extracted from DTI can characterize tumor heterogeneity and carry diagnostic values.[29] Every intratumoral voxel bears both isotropic and anisotropic diffusion information. Neither DTI-p nor DTI-q is sufficient to reflect the full tensor. This rationalizes the joint histogram analysis approach of this study. It has been previously suggested to combine DTI measures with structural images,[30] which is why the joint histogram analysis was performed in tumor regions identified on anatomical images. The results showed the Voxel Group IV ($p\uparrow/q\downarrow$) had the largest proportion in both contrast-enhancing and non-enhancing tumor regions. In this subregion, the brain microstructure is destroyed, resulting in more isotropic diffusion. There is a reduction in numbers of axons that facilitate tumor cell infiltration. The displacement and compression of fibers may also mean the 'fast track' to infiltrate is diminished and, thus, decreased anisotropic diffusion is observed. The significantly higher proportion of this diffusion pattern in the bulk tumor than the infiltrated tumor may suggest more substantial fiber damage.

More diffusion patterns can be revealed by this approach. Particularly, the higher proportion of Voxel Group II ($p\downarrow/q\uparrow$) in non-enhancing regions showed increased hazard ratio in both OS and PFS models. Since the decreased DTI-p is thought to reflect the elevated cell density and increased DTI-q may indicate intact fibers which may facilitate the tumor migration,

this subregion may represent a migratory tumor habitat. Though the proportion s relatively low, the significant association with patient survival and tumor progression may indicate its invasiveness. As shown in the case examples, some locations of this subregion is in the vicinity of the surgical cavity. Our findings may allow better targeting of radiotherapy in these subregions. Histological correlation of these findings is required.

The joint histogram features found in our study showed clinical significance, with incremental prognostic values when integrated with clinical factors. Particularly, in the model of overall survival, contrast-enhancing tumor volume had a smaller HR than all the voxel groups identified. IDH-1 mutation did not show its prognostic value in this cohort, possibly due to the limited patient numbers. As the more infiltrative subregion identified, targeted resection and radiation therapy can perhaps be achieved, which may reduce the radiation damage to the normal brain and enhance the efficacy of treatment.

There are some limitations in our study. Firstly, the patient population reported is from a single center and the results were not validated by another cohort. Secondly, although our current study did not have biological validation, previous studies have validated the histological correlates of DTI-p and DTI-q by image-guided biopsies[8]. This current study aimed to use DTI joint histogram analysis as a surrogate to investigate glioblastoma infiltration. The findings of this study need further validation using the tumor tissue biopsied from the invasive subregions identified.

Conclusion

We used a joint histogram analysis of DTI-p and -q to investigate glioblastoma infiltration. The results showed that this method may help to better understand the heterogeneity of tumor infiltration and offer incremental prognostic values over clinical factors; the non-enhancing region with decreased DTI-p and increased DTI-q may be able to define an infiltrative subregion responsible for tumor progression. This finding may be useful in targeted surgery and radiation therapy.

References

1. Ricard D, Idbaih A, Ducray F, Lahutte M, Hoang-Xuan K, Delattre JY. Primary brain tumours in adults. *Lancet.* May 26 2012;379(9830):1984-1996.

2. Weller M, van den Bent M, Tonn JC, et al. European Association for Neuro-Oncology (EANO) guideline on the diagnosis and treatment of adult astrocytic and oligodendroglial gliomas. *Lancet Oncol.* Jun 2017;18(6):e315-e329.

3. Giese A, Bjerkvig R, Berens ME, Westphal M. Cost of migration: invasion of malignant gliomas and implications for treatment. *J Clin Oncol.* Apr 15 2003;21(8):1624-1636.

4. Sottoriva A, Spiteri I, Piccirillo SGM, et al. Intratumor heterogeneity in human glioblastoma reflects cancer evolutionary dynamics. *P Natl Acad Sci USA.* Mar 5 2013;110(10):4009-4014.

5. Verhaak RGW, Hoadley KA, Purdom E, et al. Integrated Genomic Analysis Identifies Clinically Relevant Subtypes of Glioblastoma Characterized by Abnormalities in PDGFRA, IDH1, EGFR, and NF1. *Cancer Cell.* Jan 19 2010;17(1):98-110.

6. Smith CL, Kilic O, Schiapparelli P, et al. Migration Phenotype of Brain-Cancer Cells Predicts Patient Outcomes. *Cell Rep.* Jun 21 2016;15(12):2616-2624.

7. Wen PY, Macdonald DR, Reardon DA, et al. Updated Response Assessment Criteria for High-Grade Gliomas: Response Assessment in Neuro-Oncology Working Group. *J Clin Oncol.* Apr 10 2010;28(11):1963-1972.

8. Price SJ, Jena R, Burnet NG, et al. Improved delineation of glioma margins and regions of infiltration with the use of diffusion tensor imaging: An image-guided biopsy study. *Am J Neuroradiol.* Oct 2006;27(9):1969-1974.

9. Price SJ, Allinson K, Liu HX, et al. Less Invasive Phenotype Found in Isocitrate Dehydrogenase-mutated Glioblastomas than in Isocitrate Dehydrogenase Wild-Type Glioblastomas: A Diffusion-Tensor Imaging Study. *Radiology.* Apr 2017;283(1):215-221.

10. Hambardzumyan D, Bergers G. Glioblastoma: Defining Tumor Niches. *Trends Cancer.* Dec 2015;1(4):252-265.

11. Pena A, Green HAL, Carpenter TA, Price SJ, Pickard JD, Gillard JH. Enhanced visualization and quantification of magnetic resonance diffusion tensor imaging using the p : q tensor decomposition. *Brit J Radiol.* Feb 2006;79(938):101-109.

12. Price SJ, Jena R, Burnet NG, Carpenter TA, Pickard JD, Gillard JH. Predicting patterns of glioma recurrence using diffusion tensor imaging. *Eur Radiol.* Jul 2007;17(7):1675-1684.

13. Mohsen LA, Shi V, Jena R, Gillard JH, Price SJ. Diffusion tensor invasive phenotypes can predict progression-free survival in glioblastomas. *Brit J Neurosurg.* Aug 2013;27(4):436-441.

14. Parsons DW, Jones S, Zhang XS, et al. An integrated genomic analysis of human glioblastoma Multiforme. *Science.* Sep 26 2008;321(5897):1807-1812.

15. Hegi ME, Diserens A, Gorlia T, et al. MGMT gene silencing and benefit from temozolomide in glioblastoma. *New Engl J Med.* Mar 10 2005;352(10):997-1003.

16. Behrens TE, Woolrich MW, Jenkinson M, et al. Characterization and propagation of uncertainty in diffusion-weighted MR imaging. *Magn Reson Med.* Nov 2003;50(5):1077-1088.

17. Smith SM, Jenkinson M, Woolrich MW, et al. Advances in functional and structural MR image analysis and implementation as FSL. *Neuroimage.* 2004;23:S208-S219.

18. Jenkinson M, Bannister P, Brady M, Smith S. Improved optimization for the robust and accurate linear registration and motion correction of brain images. *Neuroimage.* Oct 2002;17(2):825-841.

19. Fedorov A, Beichel R, Kalpathy-Cramer J, et al. 3D Slicer as an image computing platform for the Quantitative Imaging Network. *Magn Reson Imaging.* Nov 2012;30(9):1323-1341.
20. Boonzaier NR, Larkin TJ, Matys T, van der Hoorn A, Yan JL, Price SJ. Multiparametric MR Imaging of Diffusion and Perfusion in Contrast-enhancing and Nonenhancing Components in Patients with Glioblastoma. *Radiology.* Jul 2017;284(1):180-190.
21. Dunn J, Baborie A, Alam F, et al. Extent of MGMT promoter methylation correlates with outcome in glioblastomas given temozolomide and radiotherapy. *Brit J Cancer.* Jun 30 2009;101(1):124-131.
22. Collins VP, Ichimura K, Di Y, et al. Prognostic and predictive markers in recurrent high grade glioma; results from the BR12 randomised trial. *Acta Neuropathol Com.* 2014;2.
23. Vogelbaum MA, Jost S, Aghi MK, et al. Application of novel response/progression measures for surgically delivered therapies for gliomas: Response Assessment in Neuro-Oncology (RANO) Working Group. *Neurosurgery.* Jan 2012;70(1):234-243; discussion 243-234.
24. Zhang J. Diffusion tensor imaging of white matter pathology in the mouse brain. *Imaging Med.* Dec 01 2010;2(6):623-632.
25. Price SJ, Pena A, Burnet NG, et al. Tissue signature characterisation of diffusion tensor abnormalities in cerebral gliomas. *Eur Radiol.* Oct 2004;14(10):1909-1917.
26. Sternberg EJ, Lipton ML, Burns J. Utility of Diffusion Tensor Imaging in Evaluation of the Peritumoral Region in Patients with Primary and Metastatic Brain Tumors. *Am J Neuroradiol.* Mar 2014;35(3):439-444.
27. Potgieser ARE, Wagemakers M, van Hulzen ALJ, de Jong BM, Hoving EW, Groen RJM. The role of diffusion tensor imaging in brain tumor surgery: A review of the literature. *Clin Neurol Neurosur.* Sep 2014;124:51-58.
28. Jones TL, Byrnes TJ, Yang G, Howe FA, Bell BA, Barrick TR. Brain tumor classification using the diffusion tensor image segmentation (D-SEG) technique. *Neuro-Oncology.* Mar 2015;17(3):466-476.
29. Wagner MW, Narayan AK, Bosemani T, Huisman TAGM, Poretti A. Histogram Analysis of Diffusion Tensor Imaging Parameters in Pediatric Cerebellar Tumors. *J Neuroimaging.* May-Jun 2016;26(3):360-365.
30. Bammer R. Basic principles of diffusion-weighted imaging. *Eur J Radiol.* Mar 2003;45(3):169-184.

Supplemental Digital Contents

Supplemental Digital Content 1: Pre-Operative MRI Sequences.

Supplemental Digital Content 2: Assessment of IDH-1 R132H Mutation and Methylation Status.

Supplemental Digital Content 3: Evaluation of Tumor Progression.

Supplemental Digital Content 4: Figure 1. Flowchart showing how patients were excluded.